Journal of Molecular Structure 1098 (2015) 34–40

Contents lists available at ScienceDirect

Journal of Molecular Structure

journal homepage: http://www.elsevier.com/locate/molstruc

Structural characterisation of some vanillic Mannich bases: Experimental and theoretical study

Vladimir P. Petrović [a, *], Dušica Simijonović [a], Sladjana B. Novaković [b], Goran A. Bogdanović [b], Svetlana Marković [a], Zorica D. Petrović [a]

[a] Faculty of Science, University of Kragujevac, P.O. Box 60, 34000 Kragujevac, Serbia
[b] Vinča Institute of Nuclear Sciences, University of Belgrade, P.O. Box 522, 11001 Belgrade, Serbia

ARTICLE INFO

Article history:
Received 25 February 2015
Received in revised form
28 May 2015
Accepted 29 May 2015
Available online 2 June 2015

Keywords:
Mannich bases
IR and NMR spectroscopy
Crystal structure
Density functional theory

ABSTRACT

In this paper, synthesis and structural determination of 2-[1-(*N*-4-fluorophenylamino)-1-(4-hydroxy-3-methoxyphenyl)]methylcyclohexanone (**MB-F**) is presented. To determine the structure of this new compound, IR and NMR spectral characterisation was performed experimentally and theoretically. Simulation of spectral data was carried out using three functionals: B3LYP, B3LYP-D2, and M06-2X. The results obtained for **MB-F** were compared to those attained for similar, known compound 2-[1-(*N*-phenylamino)-1-(4-hydroxy-3-methoxyphenyl)]methylcyclohexanone (**MB-H**), whose crystal structure is presented here. Taking into account all experimental and theoretical findings, the structure of **MB-F** was proposed.

1. Introduction

Mannich-type reactions are of great importance in organic synthesis. The products of these reactions are β-amino-carbonyl compounds [1–5]. Many alkaloids, nucleotides, steroids, peptides, antibiotics and vitamins [6–10] comprise Mannich base fragments. Bioactivity, such as antioxidative [11], antifungal [12], anti-inflammatory [13], antimalarial [14], vasorelaxing [15], antitubercular [16], analgesic [17], anticancer [18–21], etc., is a common feature of this class of compounds. Recently, the details on the synthesis and biological activity of some Mannich bases were reported [22]. To elucidate physico-chemical properties of compounds various methods have been developed, such as analytical techniques X-ray, NMR, IR, ESI-MS, etc., as well as quantum chemical calculations.

In this study we report the synthesis of the new Mannich base, 2-[1-(*N*-4-fluorophenylamino)-1-(4-hydroxy-3-methoxyphenyl)] methylcyclohexanone (**MB-F**). In addition we present various results related to **MB-F** and 2-[1-(*N*-phenylamino)-1-(4-hydroxy-3-methoxyphenyl)]methylcyclohexanone (**MB-H**) [22]. This investigation includes the spectroscopic and crystallographic data, as well as the results of quantum chemical calculations, and is focused towards structural determination of both compounds. Our additional goal was to test the performance of different theoretical methods in determination of structural and spectroscopic properties of the investigated Mannich bases.

2. Experimental

2.1. Reagents

The compounds chloroacetic acid, vanillin, 4-fluoroaniline, cyclohexanone, were obtained from Aldrich Chemical Co. Diethanolamine (DEA) was purchased from Fluka. All common chemicals were of reagent grade.

2.2. Measurements

The ^{1}H NMR and ^{13}C NMR spectra were run in $CDCl_3$ on a Varian Gemini 200 MHz spectrometer. The IR spectra in the solid state were recorded on a Perkin–Elmer Spectrum One FT-IR spectrometer using KBr pellet technique. The resolution of the scanning was 400 cm^{-1} at 16 scans. Melting points were determined on a Mel-Temp capillary melting points apparatus, model 1001. Elemental microanalyses for carbon, hydrogen, and nitrogen were performed at the Faculty of Chemistry, University of Belgrade.

* Corresponding author.
E-mail address: vladachem@kg.ac.rs (V.P. Petrović).

http://dx.doi.org/10.1016/j.molstruc.2015.05.040
0022-2860/

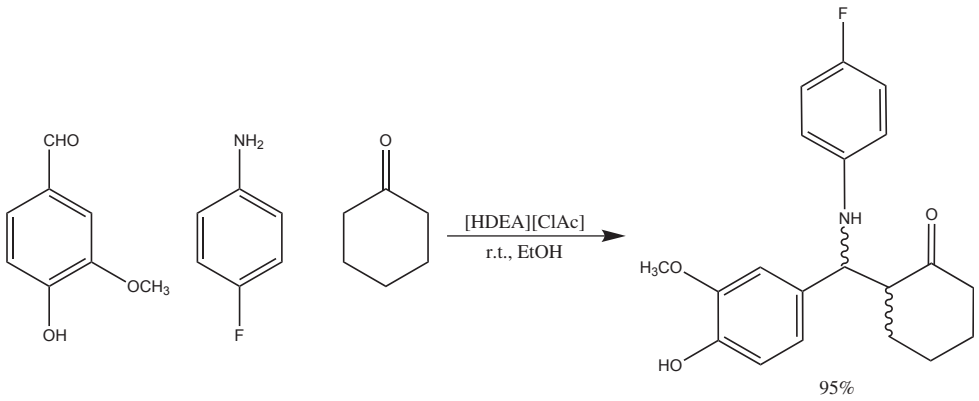

Scheme 1. Synthesis of **MB-F** with the yield indicated.

2.3. Reaction procedure

The synthesis of the Mannich product **MB-F** was performed using diethanolammonium chloroacetate [HDEA][ClAc] as catalyst (Scheme 1), whose preparation has been earlier described [22]. All components (4-fluoroaniline and vanillin (1 mmol), cyclohexanone (1.5 mmol), and ionic liquid as catalyst (15 mol%)) were stirred at room temperature for 24 h, in 1 ml of ethanol. The precipitated product was filtrated and washed with ethanol. Recrystallization from dichloromethane and propanol (2:1) yielded **MB-F**, which was analysed by ^{1}H NMR, ^{13}C NMR (Tables 2 and 3), and IR spectroscopy (Fig. 3). White compound: Mp 153–155 °C; $C_{20}H_{22}FNO_3$ (FW = 343.39): C, 69.95; N, 4.08; H, 6.46%; found: C, 70.09; N, 4.07; H, 6.20%. The synthesis of **MB-H** has been carried out using very similar procedure [22]. Possible *anti* and *syn* diastereoisomers of **MB-H** and **MB-F** are depicted in Scheme 2.

2.4. X-ray experiment

Single-crystal diffraction data for **MB-H** were collected on an Oxford Diffraction Xcalibur Sapphire3 Gemini diffractometer equipped with Cu Kα radiation (λ = 1.5418 Å) at room temperature. Data were processed with CrysAlis software [23] with multi-scan absorption corrections applied using SCALE3 ABSPACK [23]. The crystal structure was solved with SHELXS [24] and refined using SHELXL [24].

All non-H atoms were refined anisotropically to convergence. The H atoms attached to O1 and N1 were located from the difference map and were refined with isotropic displacement parameters. All H attached to C atoms were placed at geometrically calculated positions with the C–H distances fixed to 0.93 Å from C(sp^2); 0.96, 0.97 and 0.98 Å from methyl, methylene and methine C(sp^3), respectively. The positions of these H atoms were geometrically idealized and allowed to ride on their parents atoms with U_{iso}(H) = 1.2 U_{eq}(C). Methyl-group H atoms were located from Δ F map, then geometrically idealized and refined as a rigid groups with U_{iso}(H) = 1.5 U_{eq}(C).

Figures were produced using ORTEP-3 [25] and MERCURY, Version 2.4 [26]. The software used for the preparation of the materials for publication: WinGX, PLATON, PARST [27–29].

Crystallographic data for the structural analysis were deposited with the Cambridge Crystallographic Data Centre, CCDC No. 935220 for **MB-H**. These data can be obtained free of charge via www.ccdc.cam.ac.uk/data_request/cif.

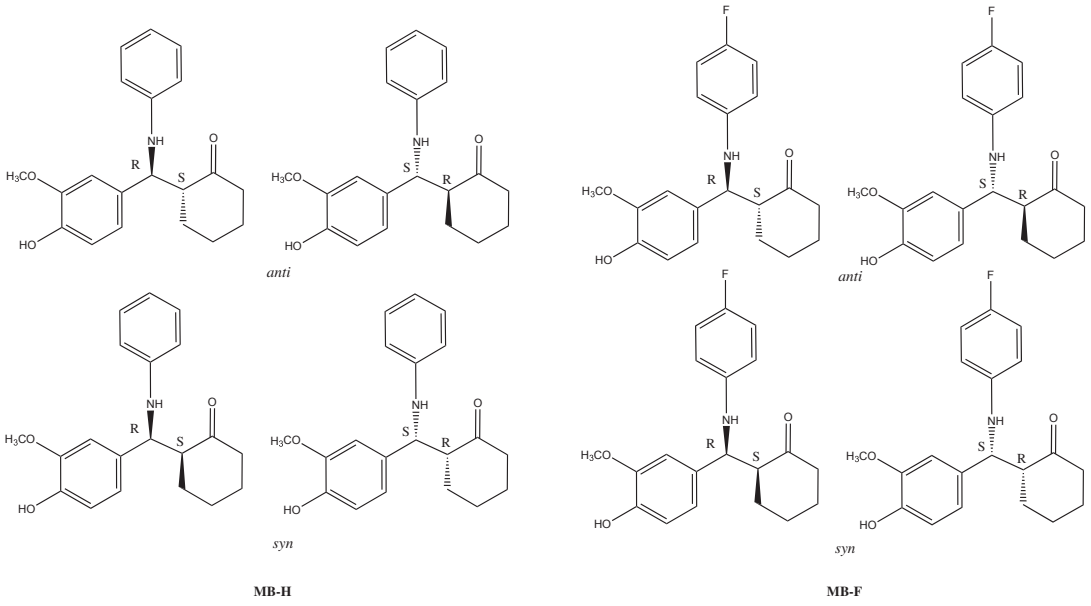

Scheme 2. Possible *RS* and *SR* enantiomers of the **MB-H** and **MB-F** diastereoisomers (*anti* and *syn*).

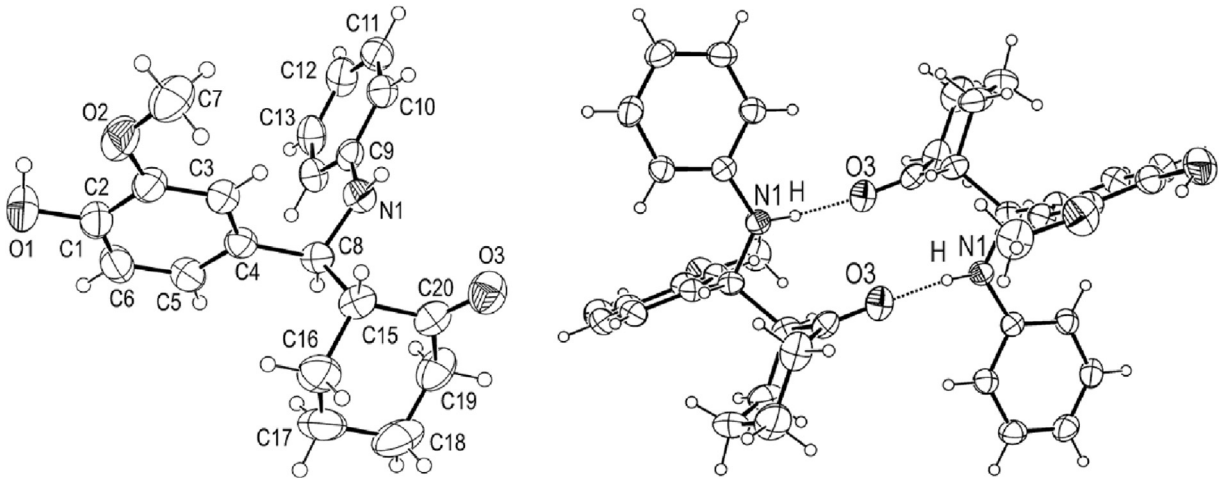

Fig. 1. Left: Molecular structure of **MB-H**. Displacement ellipsoids are drawn at the 40% probability level. The atom labelling scheme is remained throughout the paper. Right: Mutual orientation of the molecules within the dimer formed via N1–H … $O3^{i}$ hydrogen bonds [symmetry code: (i) −x+2, −y+1, −z+1]. Displacement ellipsoids are drawn at the 30% probability level.

2.5. Computational methods

All calculations were performed with the Gaussian 09 software package [30] using the B3LYP [31], B3LYP-D2 [32,33], and M06-2X [34,35] functionals in combination with the 6-311 + G(d,p) basis set. B3LYP-D2 and M06-2X were selected as widely applicable methods that proved to describe interatomic interactions at short and medium distances (≤5 Å) more accurately and reliably than traditional DFT methods. Hybrid GGA B3LYP-D2 includes an empirical correction term proposed by Grimme, whereas hybrid meta-GGA M06-2X, developed by Chao and Truhlar, is characterised by the way it has been parameterised. The structures of investigated compounds in the gas-phase and chloroform ($\varepsilon = 24.3$) were fully optimised using the conductor-like solvation model (CPCM) [36,37]. Frequency calculations were carried out to confirm that all structures are energetic minima (no imaginary vibrations). The gas-phase structures were used for examination of geometrical parameters, and predicting IR spectra. The computed frequencies were scaled by the factors of 0.950 (B3LYP), 0.955 (B3LYP-D2), and 0.945 (M06-2X). The scaling factors were obtained using the least squares method. The NMR properties of **MB-H** and **MB-F** were predicted using two procedures: default (as implemented in Gaussian) and custom. Custom procedure implies that the structures of **MB-H**, **MB-F** and TMS in chloroform were fully optimised as described above, and the NMR shifts for all hydrogen and carbon atoms relative to TMS were calculated using the Gauge-Independent Atomic Orbital (GIAO) method.

Table 1
Crystallographic data for **MB-H**.

Empirical formula	$C_{20}\,H_{23}\,N\,O_3$
Formula weight	325.39
Colour, crystal shape	Colourless, prismatic
Crystal size (mm^3)	0.48 × 0.33 × 0.23
Temperature (K)	293(2)
Wavelength (Å)	1.5418
Crystal system	Monoclinic
Space group	$P2_1/n$
Unit cell dimensions	
a (Å)	9.0772(3)
b (Å)	17.1013(7)
c (Å)	11.2214(4)
α (°)	90
β (°)	101.355(3)
γ (°)	90
V ($Å^3$)	1707.82(11)
Z	4
D_{calc} (Mg/m^3)	1.266
μ (mm^{-1})	0.679
θ range for data collection (°)	4.78 to 72.38
Reflections collected	6482
Independent reflections, R_{int}	3295, 0.0143
Completeness (%) to θ = 67°	99.9

3. Results and discussion

To our best knowledge, the crystal structure of these compounds has not been reported so far. Here we present the results of crystallographic experiment for **MB-H**. This Mannich product builds supramolecular structure with its enantiomer (Fig. 1).

A summary of crystallographic data for **MB-H** is given in Table 1, whereas experimental and calculated bond lengths, bond angles, and dihedral angles are presented in Tables S1–S3 of Supplementary material. **MB-H** contains three six-membered rings. The dihedral

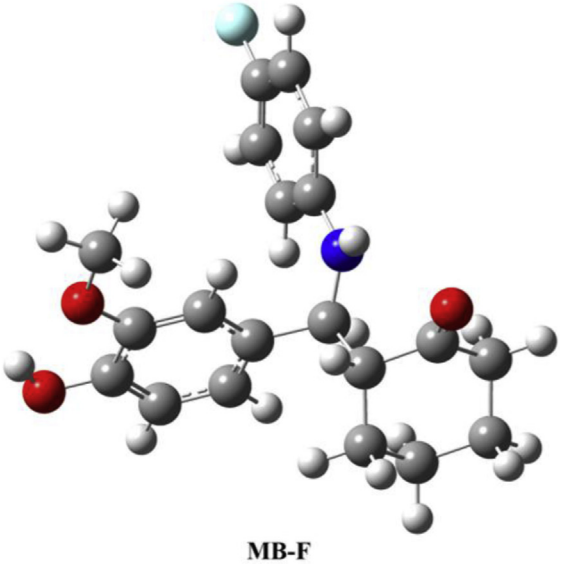

Fig. 2. Optimised geometry of 2-[1-(N-4-fluorophenylamino)-1-(4-hydroxy-3-methoxyphenyl)]methylcyclohexanone (**MB-F**).

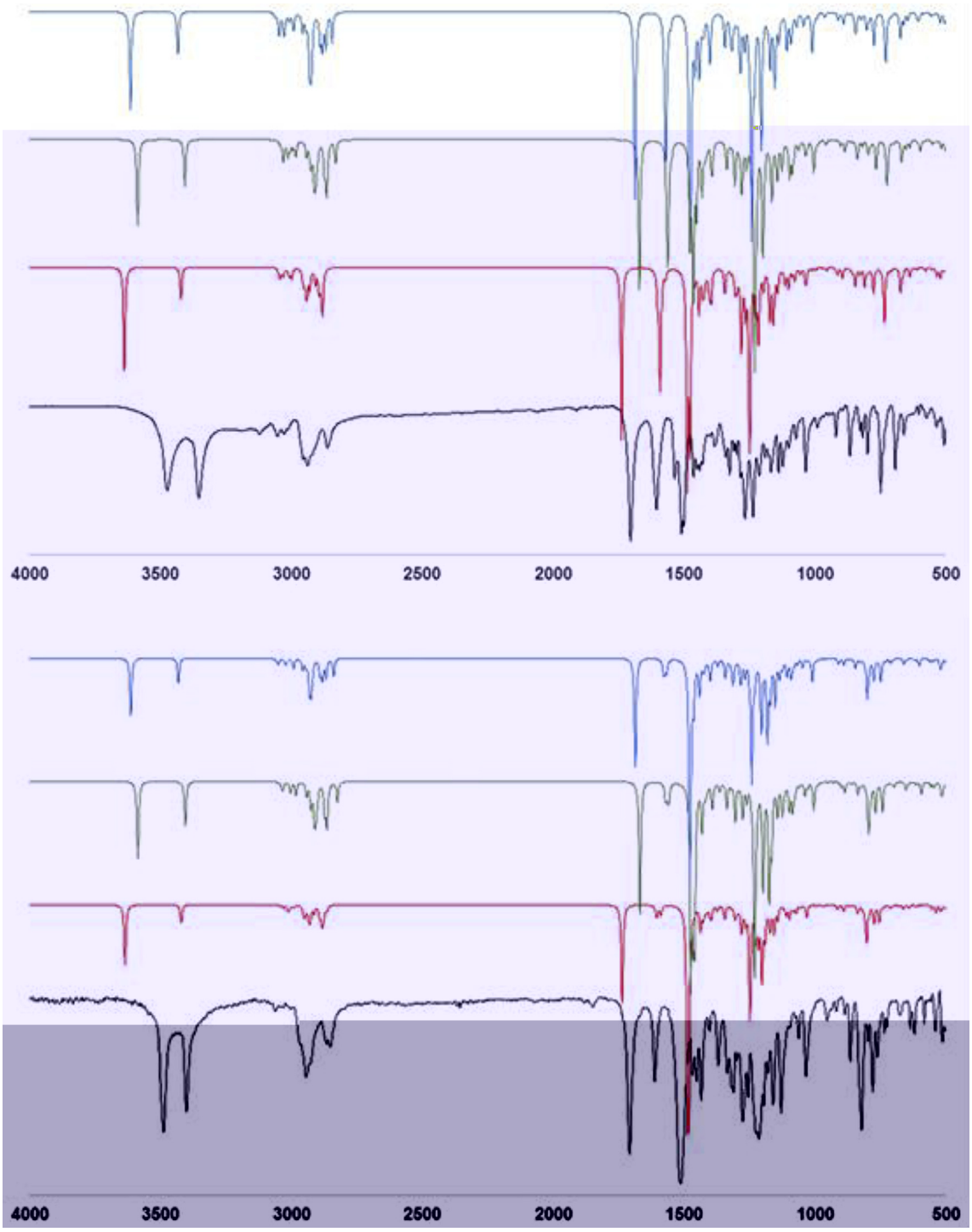

Fig. 3. Experimentally and theoretically obtained IR spectra of **MB-H** (top) and **MB-F** (bottom). Black line stands for experimental results, whereas red, green, and blue lines denote the spectra simulated with the M06-2X, B3LYP, and B3LYP-D2 methods, respectively. (For interpretation of the references to colour in this figure legend, the reader is referred to the web version of this article.)

angle between mean planes of two phenyl rings, C1–C6 and C9–C14, is 81.50(5)°. This phenyl rings are nearly orthogonally oriented to each other. The C15–C20 ring adopts an almost ideal chair conformation. The C15, C16, C18 and C19 atoms which form the base of this ring are perfectly coplanar (the root-mean-square deviation of constituent atoms from corresponding mean plane is only 0.0053 Å). The C17 and C20 atoms are displaced from the C15/C16/C18/C19 mean plane by −0.651(3) and 0.593(3) Å respectively.

The C8 atom occupies a central position in the molecule and it forms the longest C–C bond distance in **MB-H**, C8–C15 = 1.553(2) Å (Table S1). The C4–C8 and all C–C bonds within the C15–C20 ring are also single bonds with bond lengths ranging from 1.490(2) to 1.527(3) Å. The C7 methyl group is approximately coplanar to the C1–C6 phenyl ring regardless of possible rotation around the C2–O2 bond [the C3–C2–O2–C7 torsion angle is −3.6(3)°].

Two enantiomeric molecules of **MB-H** are interconnected by

Table 2
Experimental and calculated ^{1}H NMR shifts for *anti* **MB-H** and *anti* **MB-F**. Chiral carbon atoms are marked with asterisks. AAE and R stand for Average Absolute Error and correlation coefficient.

Group			CH_2		*CH–C=O		O–CH_3		N–H		*C–H		O–H		Ar–H			
Compound			MB-H	MB-F	MB-H	MB-F	MB-H	MB-F	MB-H	MB-F	MB-H	MB-F	MB-H	MB-F	MB-H		MB-F	
Experimental			2.390	2.395	2.690	2.690	2.690	2.690	2.690	2.690	2.690	2.690	2.690	2.690	7.085	6.839	6.850	6.740
			1.896	1.885											7.042	6.650	6.810	6.435
			1.837	1.640											6.882	6.557	6.850	
	MB-H	**MB-F**	1.624	1.810											6.851	6.516		
B3LYP	custom		2.395	2.392	2.690	2.655	2.690	2.655	2.690	2.655	2.690	2.655	2.690	2.655	7.251	6.678	7.184	6.620
	R		2.013	1.996											7.208	6.634	6.974	6.508
	0.996	0.994	1.829	1.674											7.141	6.566	6.878	
	AAE		1.644	1.839											6.988	6.555		
	0.14	0.1																
	default		2.405	2.382	2.690	2.655	2.690	2.655	2.690	2.655	2.690	2.655	2.690	2.655	7.269	6.636	7.186	6.686
	R		1.869	1.887											7.236	6.745	7.035	6.514
	0.994	0.992	1.783	1.624											7.181	6.637	6.931	
	AAE		1.621	1.776											7.103	6.608		
	0.19	0.12																
B3LYP-D2	custom		2.396	2.445	2.690	2.655	2.690	2.655	2.690	2.655	2.690	2.655	2.690	2.655	7.233	6.804	7.133	6.609
	R		2.016	1.974											7.113	6.622	7.030	6.514
	0.994	0.990	1.877	1.694											7.039	6.464	6.862	
	AAE		1.703	1.895											7.034	6.692		
	0.17	0.16																
	default		2.455	2.468	2.690	2.655	2.690	2.655	2.690	2.655	2.690	2.655	2.690	2.655	7.297	6.786	7.183	6.631
	R		1.914	1.912											7.145	6.758	7.091	6.540
	0.991	0.990	1.897	1.695											7.123	6.555	6.930	
	AAE		1.736	1.887											7.096	6.635		
	0.21	0.2																
M06-2X	custom		2.324	2.283	2.690	2.655	2.690	2.655	2.690	2.655	2.690	2.655	2.690	2.655	7.269	6.857	7.212	6.603
	R		1.805	1.816											7.369	6.738	6.866	6.535
	0.993	0.991	1.854	1.549											7.143	6.404	6.990	
	AAE		1.593	1.797											7.095	6.673		
	0.19	0.15																
	default		2.462	2.444	2.690	2.655	2.690	2.655	2.690	2.655	2.690	2.655	2.690	2.655	7.263	6.769	7.208	6.653
	R		1.866	1.869											7.160	6.752	7.073	6.563
	0.992	0.990	1.844	1.666											7.164	6.487	6.927	
	AAE		1.734	1.812											7.091	6.658		
	0.21	0.19																

two N1–H … O3^i hydrogen bonds [N1–H, 0.93(2) Å; N1 … O3, 2.987(2) Å; H … O3^i, 2.07(2) Å; N1–H … O3^i, 169(2)°; symmetry code: (i) −x+2,−y+1,−z+1], thus forming the centrosymmetric racemic dimer (Fig. 1). The O1–H hydroxyl group does not form any classical H-bond but it plays significant role in the intermolecular O–H … π interaction with H … C10 distance of 2.70 Å (Fig. S1). The C9–C14 phenyl rings form π … π interaction with a perpendicular interplanar distance of 3.49 Å (Fig. S2). These π … π interactions together with N1–H … O3 hydrogen bonds and O–H … π interactions form bulky layers in the crystal packing of **MB-H** (Fig. S3).

A comparison between the experimental and calculated structural parameters for **MB-H** (Tables S1–S3) shows that all theoretical methods successfully reproduced the structure of this molecule. Certainly, the solid-phase and gas-phase geometries of **MB-H** are not identical, due to the intermolecular interactions in the solid state which were ignored in the gas-phase calculations. The structure of **MB-F** was predicted using the same theoretical models (Fig. 2). The calculated geometrical parameters of this Mannich base are listed in Tables S4 – S6. To confirm the predicted structure of **MB-F** the IR and NMR spectra of **MB-H** and **MB-F** were compared, and existing differences carefully examined. In the text that follows this matter will be discussed in detail.

Experimental and simulated IR spectra of **MB-H** and **MB-F** are depicted in Fig. 3. Apparently, all levels of theory reproduced experimental spectra very well. The only deviation is observed in the case of the OH (3474 cm^{-1}) and NH (3353 cm^{-1}) stretching vibrations. All theoretical models overestimate the values for these bands, which can be attributed to the negligence of the intermolecular forces present in the solid state. The calculated spectra of **MB-H** and **MB-F** reveal the difference in their structure. Namely, in the spectrum of **MB-H** the bands at 1265 and 1234 cm^{-1} correspond to the C=O and C–H deformational vibrations. In addition to these, there is a stretching C–F vibration at 1275 cm^{-1} in the spectrum of **MB-F** (Fig. 3).

The ^{1}H and ^{13}C NMR properties of the *anti* forms of **MB-H** and **MB-F** were predicted, and the chemical shifts for all hydrogen and carbon atoms relative to TMS were calculated (Tables 2 and 3). Corresponding chemical shifts for the *syn* forms of **MB-H** and **MB-F** were also calculated, and the results are presented in Tables S7 and S8. It is important to emphasise that in the spectra of **MB-F**, as well as in the case of **MB-H**, only one diastereoisomer was observed. Inspection of Tables 2 and 3 shows that all theoretical models reproduce experimental NMR spectra of the examined compounds with satisfactory accuracy. Namely, the absolute average errors (AAE) for ^{13}C and ^{1}H NMR amount to 3–4 ppm and 0.1–0.2 ppm. In addition, the correlation coefficients (R) for the dependencies of the calculated chemical shifts on the experimental values are larger than 0.99. A comparison of the values for AAE and R in Tables 2 and 3 to those in Tables S7 and S8, leads to a conclusion that the simulated spectra of the *anti* forms of both compounds are in better agreement with the experimental spectra. Furthermore, the experimental ^{1}H NMR chemical shifts for the hydrogens bonded to the chiral carbons are in better agreement with the calculated values for the *anti* forms of both compounds. These findings are in accord with the crystal structure of **MB-H**, and demonstrate that **MB-F** also exists as *anti* isomer.

Assignation of the chemical shift values to the phenyl group protons was challenging, because they appear at similar chemical

Table 3
Experimental and calculated ^{13}C NMR shifts for *anti* **MB-H** and *anti* **MB-F**. Chiral carbon atoms are marked with asterisks. AAE and R stand for Average Absolute Error and correlation coefficient.

Group			CH_2		$CH_2-C=O$		OCH_3		*CH−N		*CH−C=O		Ar−H				C=O	
Compound			MB-H	MB-F	MB-H	MB-F	MB-H	MB-F	MB-H	MB-F	MB-H	MB-F	MB-H		MB-F		MB-H	MB-F
Experimental					40.535	41.770	55.776	55.880	55.776	58.800	56.702	57.620	148.235	115.870	146.810	115.150	211.425	213.100
			38.858	31.160									147.605	115.028	144.770	115.150		
			30.619	27.830									133.077	113.283	143.650	114.860		
			22.804	23.620									128.611	111.599	133.410	114.720		
													120.225	113.283	120.490	114.070		
													120.225	111.599	115.590	109.250		
B3LYP	custom				41.316	41.444	53.541	53.661	57.621	57.386	61.267	60.430	143.651	120.478	153.734	113.031	212.043	212.075
	R		31.999	31.662									143.396	113.252	143.722	112.683		
	0.995	0.996	31.234	31.389									143.043	111.723	142.687	112.108		
	AAE		23.604	23.649									130.436	109.019	140.404	109.381		
	3.79	3.41											126.146	107.284	130.401	107.843		
													125.800	102.658	120.664	102.796		
	default				39.417	39.902	52.635	52.756	57.467	57.542	60.231	60.070	144.630	120.818	155.608	113.586	209.047	212.075
	R		30.526	29.764									144.134	114.467	144.697	112.953		
	0.995	0.995	30.417	30.233									144.907	111.719	144.869	111.918		
	AAE		22.806	23.169									131.365	109.592	140.524	110.016		
	3.95	3.75											126.580	107.874	131.229	107.918		
													126.295	101.637	120.789	101.837		
B3LYP-D2	custom				40.830	40.832	53.416	53.465	57.024	57.026	57.024	60.228	143.825	119.325	153.480	113.020	212.272	211.922
	R		32.437	32.503									143.077	113.480	143.701	112.441		
	0.996	0.996	31.816	31.881									142.053	111.745	142.481	112.384		
	AAE		23.733	24.006									130.663	110.056	140.339	110.287		
	3.48	3.33											125.788	108.978	129.759	109.595		
													125.707	102.557	119.481	102.632		
	default				39.277	38.888	53.145	52.895	57.236	57.502	57.236	59.719	145.135	119.182	155.569	113.384	208.930	208.470
	R		30.791	30.874									143.649	114.578	144.977	113.012		
	0.995	0.996	31.206	31.248									144.339	111.719	144.479	111.913		
	AAE		23.475	23.864									130.926	110.845	140.274	111.307		
	3.64	3.52											126.290	109.509	130.280	109.744		
													126.278	101.722	119.599	101.834		
M06-2X	custom				38.424	38.349	48.374	47.721	53.084	52.193	56.575	56.095	140.754	121.982	148.410	115.331	209.975	210.472
	R		27.237	28.259									142.753	116.059	140.285	115.057		
	0.995	0.996	28.405	27.719									140.067	114.349	139.059	114.445		
	AAE		20.500	19.898									132.124	111.948	138.475	112.669		
	4.23	3.56											128.033	112.033	131.089	112.123		
													127.882	105.085	122.269	104.925		
	default				39.363	38.985	52.169	51.923	57.835	57.920	60.353	60.323	144.789	119.910	154.931	113.191	208.480	208.197
	R		30.228	30.241									144.076	114.184	144.530	112.801		
	0.995	0.996	30.435	30.523									144.135	112.039	144.261	112.387		
	AAE		23.464	23.461									130.895	109.939	140.433	110.742		
	3.76	3.57											126.556	111.054	130.559	110.564		
													125.948	101.743	120.368	101.873		

shifts, and partially overlap. Due to electron donor nature of fluorine, the protons from the aniline moiety of **MB-F** appeared at somewhat lower chemical shifts, in comparison to the corresponding protons in **MB-H**. The same influence of the fluorine electric field to the corresponding carbon atoms was observed in the ^{13}C NMR spectra (Tables 2 and 3, S7, and S8). It should be emphasised that all theoretical models successfully reproduced this occurrence.

4. Conclusion

A novel compound 2-[1-(*N*-4-fluorophenylamino)-1-(4-hydroxy-3-methoxyphenyl)]methylcyclohexanone (**MB-F**) was synthesised. The structure of the similar compound 2-[1-(*N*-phenylamino)-1-(4-hydroxy-3-methoxyphenyl)]methylcyclohexanone (**MB-H**) in the crystalline phase was determined by X-ray experiment. In addition, the IR and NMR spectra of both compounds were determined experimentally. Theoretical examination of **MB-H** and **MB-F** was carried out to support experimental results. Namely, the molecular geometries were optimised, and the IR and NMR spectra simulated using three density functional methods. Taking into account that very good agreement between experimental and theoretical results was achieved, the structure of **MB-F** was proposed.

Acknowledgement

This work is supported by the Ministry of Education, Science and Technological Development of Serbia, project Nos 172016 and 172035.

Appendix A. Supplementary data

Supplementary data related to this article can be found at http://dx.doi.org/10.1016/j.molstruc.2015.05.040.

References

[1] C. Mannich, W. Krösche, Arch. Pharm. 250 (1912) 647–667.
[2] S. Sahoo, T. Joseph, S.B. Halligudi, J. Mol. Catal. A Chem. 244 (2006) 179–182.
[3] M. Shiri, Chem. Rev. 112 (2012) 3508–3549.
[4] R. Muller, H. Goesmann, H. Waldmann, Angew. Chem. Int. Ed. 38 (1999) 184–187.
[5] M. Arend, B. Westermann, N. Risch, Angew. Chem. 110 (1998) 1096–1122.
[6] B.B. Toure, D.G. Hall, Chem. Rev. 109 (2009) 4439–4486.
[7] M. Arend, B. Westermann, N. Risch, Angew. Chem. Int. Ed. 37 (1998) 1044–1070.
[8] A. Izumiseki, K. Yoshida, A. Yanagisawa, Org. Lett. 11 (2009) 5310–5313.
[9] A. Córdova, Acc. Chem. Res. 37 (2004) 102–112.
[10] S.N. Pandeya, V.S. Lahshmi, A. Pandeya, Indian. J. Pharm. Sci. 65 (2002) 213–222.
[11] D.H. Park, J. Venkatesan, S.K. Kim, V. Ramkumar, P. Parthiban, Bioorg. Med. Chem. Lett. 22 (2012) 6362–6367.
[12] H.I. Gul, T. Ojanen, J. Vepsalainen, M. Gul, E. Erciyas, O. Hanninen, Arzneimittelforschung 51 (2001) 72–75.
[13] M. Kouskoura, D. Hadjipavlou-Litina, M. Giakoumakou, Med. Chem. 4 (2008) 586–596.
[14] F. Lopes, R. Capela, J.O. Goncaves, P.N. Horton, M.B. Hursthouse, J. Iley, C.M. Casimiro, J. Bom, R. Moreira, Tetrahedron Lett. 45 (2004) 7663–7666.
[15] M.G. Ferlin, G. Chiarelotto, F. Antonucci, L. Caparrotta, G. Froldi, Eur. J. Med. Chem. 37 (2002) 427–434.
[16] S. Joshi, N. Khosla, P. Tiwari, Bioorg. Med. Chem. 12 (2004) 571–576.
[17] W. Malinka, P. Swiatek, B. Filipek, J. Sapa, A. Jerierska, A. Koll, Farmaco 60 (2005) 961–968.
[18] B.S. Holla, B. Veerendra, M.K. Shivananda, B. Poojary, Eur. J. Med. Chem. 38 (2003) 759–767.
[19] K. Kucukoglu, M. Gul, M. Atalay, E. Mete, C. Kazaz, O. Hanninen, H.I. Gul, Arzneimittelforschung 61 (2011) 366–371.
[20] H.I. Gul, J. Vepsalainen, M. Gul, E. Erciyas, O. Hanninen, Pharm. ActaHelv 74 (2000) 393–398.
[21] J.R. Dimmock, E. Erciyas, S.K. Raghavan, D.L. Kirkpatrick, Pharmazie 45 (1990) 755–757.
[22] V.P. Petrović, D. Simijonović, M.N. Živanović, J.V. Košarić, Z.D. Petrović, S. Marković, S.D. Marković, RSC Adv. 4 (2014) 24635–24644.
[23] Oxford Diffraction, CrysAlis CCD and CrysAlis RED, Versions 1.171.32.24, Oxford Diffraction Ltd., Abington, England, 2008.
[24] G.M. Sheldrick, Acta Crystallogr. Sect. A 64 (2008) 112–122.
[25] L.J. Farrugia, J. Appl. Crystallogr. 30 (1997) 565–566.
[26] C.F. Macrae, P.R. Edgington, P. McCabe, E. Pidcock, G.P. Shields, R. Taylor, M. Towler, J. van de Streek, J. Appl. Crystallogr. 39 (2006) 453–457.
[27] L.J. Farrugia, G.X. Win, J. Appl. Cryst. 32 (1999) 837–838.
[28] A.L. Spek, J. Appl. Crystallogr. 36 (2003) 7–13.
[29] M. Nardelli, J. Appl. Crystallogr. 28 (1995), 659–659.
[30] M.J. Frisch, W.G. Trucks, B.H. Schlegel, E.G. Scuseria, A.M. Robb, R.J. Cheeseman, G. Scalmani, V. Barone, B. Mennucci, A.G. Petersson, H. Nakatsuji, M. Caricato, X. Li, P.H. Hratchian, F.A. Izmaylov, J. Bloino, G. Zheng, L.J. Sonnenberg, M. Hada, M. Ehara, K. Toyota, R. Fukuda, J. Hasegawa, M. Ishida, T. Nakajima, Y. Honda, O. Kitao, H. Nakai, T. Vreven, A.J. Montgomery Jr., A.J. Montgomery Jr., E.J. Peralta, F. Ogliaro, M. Bearpark, J.J. Heyd, E. Brothers, N.K. Kudin, N.V. Staroverov, R. Kobayashi, J. Normand, K. Raghavachari, A. Rendell, C.J. Burant, S.S. Iyengar, J. Tomasi, M. Cossi, N. Rega, M.J. Millam, M. Klene, E.J. Knox, B.J. Cross, V. Bakken, C. Adamo, J. Jaramillo, R. Gomperts, E.R. Stratmann, O. Yazyev, J.A. Austin, R. Cammi, C. Pomelli, W.J. Ochterski, L.R. Martin, K. Morokuma, G.V. Zakrzewski, A.G. Voth, P. Salvador, J.J. Dannenberg, S. Dapprich, D.A. Daniels, O. Farkas, B.J. Foresman, V.J. Ortiz, J. Cioslowski, J.D. Fox, Gaussian 09, Rev A.1, Gaussian Inc, Wallingford, 2009.
[31] A.D. Becke, Density-functional thermochemistry. III. The role of exact exchange, J. Chem. Phys. 98 (1993) 5648–5652.
[32] S. Grimme, J. Comp. Chem. 25 (2004) 1463–1473.
[33] S. Grimme, J. Comp. Chem. 27 (2006) 1787–1799.
[34] Y. Zhao, D.G. Truhlar, Theor. Chem. Acc. 120 (2008) 215–241.
[35] Y. Zhao, D.G. Truhlar, Acc. Chem. Res. 41 (2008) 157–167.
[36] V. Barone, M. Cossi, J. Phys. Chem. A 102 (1998) 1995–2001.
[37] M. Cossi, N. Rega, G. Scalmani, V. Barone, J. Comput. Chem. 24 (2003) 669–681.